N-Methyl-*N*-alkylpyrrolidinium Hexafluorophosphate Salts: Novel Molten Salts and Plastic Crystal Phases

J. Golding,[†] N. Hamid,[†] D. R. MacFarlane,*[,†] M. Forsyth,[‡] C. Forsyth,[†] C. Collins,[†,‡] and J. Huang[†]

Department of Chemistry, Monash University, Clayton, Victoria, 3800 Australia, and Department of Materials Engineering, Monash University, Clayton, Victoria, 3800 Australia

Received July 28, 2000. Revised Manuscript Received November 15, 2000

A new series of salts, based on the *N*-methyl-*N*-alkylpyrrolidinium cation and the PF_6^- anion, are reported and their thermal properties described for alkyl = Me, Et, Pr, Bu, Hx, and Hp. X-ray structures of several of the salts are also reported. The *N*,*N*-dimethylpyrrolidinium hexafluorophosphate has a melting point greater than 390 °C; however, the *N*-methyl-*N*-butylpyrrolidinium derivative melts at 70 °C. Most of the PF_6^- salts were observed to have lower melting points in comparison with the analogous iodide salts. Most of the salts exhibit one or more thermal transitions prior to melting and a final entropy of melting less than 20 J K^{-1} mol^{-1}, behavior which has previously been associated with the formation of plastic crystal phases. Good crystal structure solutions were obtained at low temperatures in the case of the alkyl = propyl and heptyl derivatives. The loss of diffraction peaks and changes in symmetry at higher temperatures indicated the presence of dynamic rotational disorder, supporting the understanding that the plastic properties arise from rotational motions in the crystal.

Introduction

There are many physical forms that an electrolyte can take including molten salt, solvent-based solution, polymer-based solution, crystalline, and amorphous solid.[1] In solvent-based systems, the solvent (either liquid or polymer) dissociates the solute into free ions. Disadvantages associated with the solvent-based electrolytes in battery applications include corrosion, leakage, and the fact that the solvent molecules, to some extent, impede the motion of the free ions.[2] Ionic liquids, or molten salts, have many desirable properties; in their liquid state they are generally good conductors, and in many cases they possess a wide electrochemical window and high thermal stability.[3,4] Molten organic salts such as those based on the imidazolium, pyrrolidinium, and quaternary ammonium cations have been of interest for their use in a variety of electrochemical applications, as well as for ionic media/solvents for organic reactions and spectroscopic analysis.[5,6] Thus significant efforts have been devoted recently to the preparation of low melting point ionic materials.[5−11]

Recently, a number of small chain length, alkylmethylpyrrolidinium compounds (**I**)

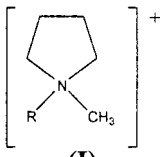

(I)

with low melting points have been prepared by associating the organic cation with very weakly basic anions.[6] Weakly complexing anions, including $(CF_3SO_2)_2N^-$, BF_4^-, $CF_3SO_3^-$, PF_6^-, and CH_3COO^-, possess a negative charge which is either strongly delocalized over a number of atoms or is shielded by a shell of other atoms. Such anions therefore cannot participate in strong ionic interactions with the cation. One manifestation of the weak ionic interactions in these salts is a generally lower melting point compared to anions which interact strongly, e.g. Cl^-.[7] It has been reported[6,8,9] that the $(CF_3SO_2)_2N^-$ anion depresses the melting point by as much as 100 °C for this reason, as compared with analogous halide compounds. For example, *N*-methyl-*N*-propylpyrrolidinium bis(trifluoromethylsulfonyl)amide has a melting point of −14 °C as compared with the iodide of the same cation, melting point = 113 °C.[6]

It has also been discovered recently[6] that amide salts in the pyrrolidinium family can exhibit ion conduction

* To whom correspondence should be addressed.
[†] Department of Chemistry.
[‡] Department of Materials Engineering.

(1) Forsyth, M.; MacFarlane, D. R. *Wiley Encycl. Electr. Electron. Eng.* **1999**, *6*, 408−418.
(2) Archuleta, M. M. *J. Power Sources* **1995**, *54*, 138−142.
(3) Sun, J.; Forsyth, M.; MacFarlane, D. R. *J. Phys. Chem.* **1998**, *102*, 8858.
(4) Bonhote, P.; Dias, A.-P.; Papageorgiou, N.; Kalyanasundaram, K.; Gratzel, M. *Inorg. Chem.* **1996**, *35*, 1168.
(5) Seddon, K. R. *J. Chem. Technol. Biotech.* **1997**, *68*, 351.
(6) MacFarlane, D. R.; Meakin, P.; Sun, J.; Amini, N.; Forsyth, M. *J. Phys. Chem. B* **1999**, *103*, 4164−4170.
(7) Fuller, J.; Carlin, R. T.; Long, H. C. D.; Haworth, D. *Chem. Commun.* **1994**, 299.
(8) Bonhote, P.; Dias, A.-P.; Papageorgiou, N.; Kalyanasundaram, K.; Gratzel, M. *Inorg. Chem.* **1996**, *35*, 1168.
(9) Golding, J. J.; MacFarlane, D. R.; Spiccia, L.; Forsyth, M. *J. Chem. Soc., Chem. Commun.* **1998**, *15*, 1593.
(10) MacFarlane, D. R.; Huang, J.; Forsyth, M. *Nature* **1999**, 402.
(11) Forsyth, M.; Huang, J.; MacFarlane, D. R. *J. Mater. Chem.* **2000**, *10*, 2259−2265.

10.1021/cm000625w CCC: $20.00
Published on Web 01/23/2001

in the solid state due to the presence of plastic crystal phases. Doping these salts with lithium salts of the same anion leads to increases in conductivity of up to 2 orders of magnitude.[10,11] This observation indicates that these interesting doped compounds can be considered as new members of the family of fast-ion conducting materials. Fast-ion conductors are characterized by the rapid movement of one ion within a relatively static matrix of other ions or molecular species. Conductivities observed thus far are sufficiently high that the doped plastic crystal phases are of interest in practical lithium batteries, and thus, we have began to investigate other related members of the pyrrolidinium salt family in this case the PF_6^- salts.

The plastic crystal and diffusional properties found in the pyrrolidinium salts, which lead to high intrinsic ionic conductivity, are most likely related to structural order/disorder within the crystalline lattice as observed by Ikeda and co-workers[12−16] for a number of ammonium compounds. Thus the nature of the cation/anion packing within the lattice, as well as the interatomic distances and interaction strengths, will influence the transport properties of these materials. To further understand the structure−property relationships in the pyrrolidinium family of plastic crystals, chemical variations have been investigated including alkyl length substitution and anion type. In this paper particular emphasis is given to thermal and crystallographic analysis of a family of alkyl-substituted pyrrolidinium salts. Due to the inherent rotational disorder and metastable thermal behavior often observed in plastic crystal materials, single crystal diffraction data has generally been difficult to obtain. However, in this work we describe the preparation and full X-ray structural characterization of a family of pyrrolidinium plastic crystals based on the PF_6^- anion.

Experimental Section

The various alkyl iodides (Aldrich/BDH/Fluka), potassium hexafluorophosphate (KPF_6, Aldrich), 1-methylpyrrolidine (Aldrich), and *i*-PrOH (BDH) were used as received. Melting points were measured using an uncalibrated capillary tube apparatus and were obtained as ranges from the visual observation of onset to completion of the melt or decomposition. This information was used to guide the methodology for the differential scanning calorimetry. Differential scanning calorimetry (DSC) was carried out on an accurately known mass of sample sealed in an Al DSC pan under an inert atmosphere using a Perkin-Elmer DSC-7 with ambient temperatures and above (50−200 °C) calibrated with respect to power and temperature with indium (156.54 °C) and *p*-nitrotoluene (51.64 °C); subambient temperatures were calibrated with cyclohexane (s−s at −87.06 °C and melting at 6.54 °C). Transitions recorded are peak maximum temperatures. Entropies of fusion were determined from the calibrated thermogram peak areas and the relationship $\Delta S_f = \Delta H_f/T_m$, where ΔS_f and ΔH_f are the molar entropy and enthalpy of fusion respectively and T_m is the melting point. Glass transition temperatures, T_g, are recorded at the onset of the transition. ^{1}H, ^{19}F, ^{13}C, and ^{31}P NMR spectra were recorded on a Bruker DPX-300 MHz spectrometer, in DMSO-d_6. Tetramethylsilane (TMS) and trifluorochloromethane were used as internal standards. Infrared spectra were obtained on an Perkin-Elmer FTIR 1600 instrument. Samples were crushed with potassium bromide (as approximately 5% of sample by mass of KBr) and pressed into disks. Electrospray mass spectroscopy was carried out on a Micromass Platform with an electrospray source. Samples were dissolved in methanol, and both positive and negative species were detected.

Synthesis and Characterization. The *N*-alkyl-*N*-methylpyrrolidinium iodides were initially synthesized according to literature methods;[6,17] however, a modified procedure using *i*-PrOH as the solvent was found to give equally good results:

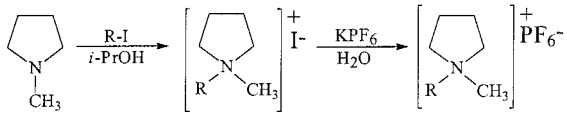

Salts were prepared having R = methyl, ethyl, propyl, butyl, hexyl, and heptyl. For simplicity the cation nomenclature is abbreviated to P_{1x}, where P indicates the pyrrolidinium cation, the subscript 1 indicates the *N*-methyl substituent, and subscript *x* indicates the carbon number of the other *N*-alkyl substituent. For example the *N*-methyl-*N*-propylpyrrolidinium cation is denoted P_{13}. Metathesis for all salts utilized the following method: A slight excess of potassium hexafluorophosphate, KPF_6, and the *N*-alkyl-*N*-methylpyrrolidinium iodide were dissolved separately in a minimum of distilled water. These solutions were then mixed together, stirred for approximately 1 h, and washed three times with water. The precipitated solid was filtered out and dried in vacuo for 2 days. The supernatant liquid was allowed to reduce in volume by slow evaporation, producing single crystals of quality suitable for X-ray analysis.

N,N-Dimethylpyrrolidinium Hexafluorophosphate ($P_{11}PF_6$). A 3.12 g amount (14 mmol) of $P_{11}I$ and 2.52 g (14 mmol) of KPF_6 yielded 2.36 g of $P_{11}PF_6$ (yield 70%). IR: 3056, 2991, 2922, 1480, 1415, 1308, 1279, 1251, 1128, 1004, 978, 936, 831, 558 cm^{-1}. ^{1}H NMR (300 MHz, DMSO-d_6): δ 2.09 (br-m, 2 × CH_2), 3.07 (s, 2 × CH_3), 3.44 (br-t, 2 × CH_2) ppm. ^{19}F NMR (282 MHz, DMSO-d_6): δ −69.49 ppm (d, 6F). ^{13}C NMR (75 MHz, DMSO-d_6): δ 21.35 (s, 2 × CH_2), 51.00 (t, 2 × CH_3), 64.78 (t, 2 × CH_2) ppm. Electrospray MS (*m*/*z*): ES+ 99.7 (100% − P_{11}^+), 345.2 (5% − $[(P_{11})_2PF_6]^+$); ES− 144.8 (100% − PF_6^-). Anal. Calcd: C, 29.38; H, 5.71; N, 5.71. Found: C, 29.25; H, 5.66; N, 5.55.

N-Ethyl-N-methylpyrrolidinium Hexafluorophosphate($P_{12}PF_6$). A 3.30 g amount (14 mmol) of $P_{12}I$ and 2.52 g (14 mmol) of KPF_6 yielded 2.34 g of $P_{12}PF_6$ (yield 66%). IR: 3004, 2907, 1475, 1433, 1407, 1367, 1344, 1304, 1236, 1112, 1039, 998, 864, 557 cm^{-1}. ^{1}H NMR (300 MHz, DMSO-d_6): δ 1.27 (br-t, CH_3), 2.07 (br-t, 2 × CH_2), 2.95 (s, CH_3), 3.36 (q, CH_2), 3.42 (br-m, 2 × CH_2) ppm. ^{19}FNMR (282 MHz, DMSO-d_6): δ −69.47 (d, 6F) ppm. ^{13}C NMR (75 MHz, DMSO-d_6): δ 7.75 (s, CH_3), 20.08 (s, 2 × CH_2), 45.96 (t, CH_3), 57.43 (d, CH_2), 61.93 (t, 2 × CH_2) ppm. ^{31}P NMR (121 MHz, DMSO-d_6): δ 144.58 (m, 1P) ppm. Electrospray MS (*m*/*z*): ES+ 113.9 (100% − P_{12}^+), 114.9 (8% − P_{12}^+), 373.5 (5% − $[(P_{12})_2PF_6]^+$); ES− 144.8 (100% − PF_6^-).

N-Propyl-N-methylpyrrolidinium Hexafluorophosphate($P_{13}PF_6$). A 3.50 g amount (14 mmol) of $P_{13}I$ and 2.51 g (14 mmol) of KPF_6 yielded 2.17 g of $P_{13}PF_6$ (yield 58%). IR: 2984, 2893, 1626, 1572, 1474, 1406, 1365, 1240, 1122, 1044, 1005, 836, 557 cm^{-1}. ^{1}H NMR (300 MHz, DMSO-d_6): δ 0.92 (t, CH_3), 1.72 (m, CH_2), 2.08 (br-t, 2 × CH_2), 2.97 (s, CH_3), 3.24 (q, CH_2), 3.43 (br-m, 2 × CH_2) ppm. ^{19}F NMR (282 MHz, DMSO-d_6): δ −69.52 (d, 6F) ppm. ^{13}C NMR (75 MHz, DMSO-d_6): δ 10.57 (s, CH_3), 16.50 (s, CH_2), 21.06 (s, 2 × CH_2), 47.55 (t, CH_3), 63.43 (t, 2 × CH_2), 64.51 (s, CH_2) ppm. Electrospray MS (*m*/*z*): ES+

(12) Ono, H.; Ishimaru, S.; Ikeda, R.; Ishida, H. *Bull. Chem. Soc. Jpn.* **1999**, *72*, 2049−2054.
(13) Hattori, M.; Fukuda, S.; Nakamura, D.; Ikeda, R. *J. Chem. Soc., Faraday Trans.* **1990**, *86*, 3777.
(14) Iwai, S.; Hattori, M.; Nakamura, D.; Ikeda, R. *J. Chem. Soc., Faraday Trans.* **1993**, *89*, 827.
(15) Tanabe, T.; Nakamura, D.; Ikeda, R. *J. Chem. Soc., Faraday Trans.* **1991**, *87*, 987−900.
(16) Shimizu, T.; Tanaka, S.; Onoda-Yamamuro, N.; Ishimaru, S.; Ikeda, R. *J. Chem. Soc., Faraday Trans.* **1997**, *93* (2), 321−326.
(17) Sun, J.; Forsyth, M.; MacFarlane, D. R. *Ionics* **1997**, *3*, 356.

Table 1. Thermal Properties of *N*-Alkyl-*N*-methylpyrrolidinium (P_{1x}) Hexafluorophosphate Salts

acronym	$T_{IV\rightarrow III}$ (±2 °C)	$T_{III\rightarrow II}$ (±2 °C)	$T_{II\rightarrow I}$ (±2 °C)	MP (±2 °C)	ΔS_f (J K^{-1} mol^{-1}) (±5%)
$P_{11}PF_6$			−50	~**390 (dec)**	
$P_{12}PF_6$	−70	−30	80	200	
$P_{13}PF_6$	−97	82	97	113	17
$P_{14}PF_6$		14	43	70	13
$P_{16}PF_6$			−15	203	18
$P_{17}PF_6$				66	34

127.7 (100% − P_{13}^+), 128.7 (10% − P_{13}^+), 401.5 (5% − $[(P_{13})_2PF_6]^+$); ES− 144.8 (100% − PF_6^-).

N-Butyl-N-methylpyrrolidinium Hexafluorophosphate ($P_{14}PF_6$). A 3.70 g amount (14 mmol) of $P_{14}I$ and 2.55 g (14 mmol) KPF_6 yielded 2.59 g of $P_{14}PF_6$ (yield 65%). IR: 2970, 2881, 1621, 1579, 1543, 1476, 1436, 1405, 1305, 1242, 1123, 1063, 1005, 931, 839, 741, 558 cm^{-1}. ^{1}H NMR (300 MHz, DMSO-d_6): δ 0.92 (t, CH_3), 1.31 (m, CH_2), 1.67 (m, CH_2), 2.06 (br-t, 2 × CH_2), 2.96 (s, CH_3), 3.24 (q, CH_2), 3.43 (br-m, 2 × CH_2) ppm. ^{19}F NMR (282 MHz, DMSO-d_6): δ −69.47 (d, 6F) ppm. ^{13}C NMR (75 MHz, DMSO-d_6): δ 13.81 (s, CH_3), 19.65 (s, 2 × CH_2), 21.47 (s, CH_2), 25.27 (s, CH_2), 47.93 (t, CH_3), 63.32 (s, CH_2), 63.81 (t, 2 × CH_2) ppm. Electrospray MS (*m*/*z*): ES+ 141.7 (100% − P_{14}^+), 142.7 (10% − P_{14}^+), 429.4 (5% − $[(P_{14})_2PF_6]^+$); ES− 144.8 (100% − PF_6^-).

N-Hexyl-N-methylpyrrolidinium Hexafluorophosphate ($P_{16}PF_6$). A 4.10 g amount (14 mmol) of $P_{16}I$ and 2.60 g (14 mmol) of KPF_6 yielded 2.73 g of $P_{16}PF_6$ (yield 62.3%). IR 2965, 2935, 2865, 1720, 1703, 1580, 1472, 1435, 1404, 1384, 1344, 1306, 1239, 1055, 997, 834, 735, 558 cm^{-1}. ^{1}H NMR (300 MHz, DMSO-d_6): δ 0.88 (t, CH_3), 1.29 (m, 3 × CH_2), 1.68 (m, CH_2), 2.08 (br-t, 2 × CH_2), 2.96 (s, CH_3), 3.27 (m, CH_2), 3.42 (br-m, 2 × CH_2) ppm. ^{19}F NMR (282 MHz, DMSO-d_6): δ −69.48 (d, 6F) ppm. ^{13}C NMR (75 MHz, DMSO-d_6): δ 14.16 (s, CH_3), 21.46 (s, 2 × CH_2), 22.21 (s, CH_2), 23.21 (s, CH_2), 25.91 (s, CH_2), 31.00 (s, CH_2), 47.91 (t, CH_3), 63.52 (s, CH_2), 63.81 (t, 2 × CH_2) ppm. Electrospray MS (*m*/*z*): ES+ 169.9 (100% − P_{16}^+), 171.0 (10% − P_{16}^+), 485.4 (5% − $[(P_{16})_2PF_6]^+$); ES− 144.8 (100% − PF_6^-), 460.2 (5% − $[P_{16}(PF_6)_2]-$).

N-Heptyl-N-methylpyrrolidinium Hexafluorophosphate ($P_{17}PF_6$). A 4.25 g amount (14 mmol) of $P_{17}I$ and 2.55 g (14 mmol) of KPF_6 yielded $P_{17}PF_6$ (yield 72%). IR: 3063, 2966, 2924, 2858, 1638, 1476, 1441, 1408, 1380, 1308, 1235, 1004, 934, 839, 728, 558 cm^{-1}. ^{1}H NMR (300 MHz, DMSO-d_6): δ 0.83 (t, CH_3), 1.25 (br-m, 4 × CH_2), 1.67 (m, CH_2), 2.03 (br-t, 2 × CH_2), 2.92 (s, CH_3), 3.24 (m, CH_2), 3.40 (br-m, 2 × CH_2) ppm. ^{19}F NMR (282 MHz, DMSO-d_6): δ −69.47 (d, 6F) ppm. ^{13}C NMR (75 MHz, DMSO-d_6): δ 14.83 (s, CH_3), 22.08 (s, 2 × CH_2), 22.94 (s, CH_2), 23.90 (s, CH_2), 26.84 (s, CH_2), 29.11 (s, CH_2), 31.98 (s, CH_2), 48.53 (t, CH_3), 64.18 (s, CH_2), 63.44 (t, 2 × CH_2) ppm. Electrospray MS (*m*/*z*): ES+ 184.2 (100% − P_{17}^+), 185.1 (10% − P_{17}^+), 513.6 (5% − $[(P_{17})_2PF_6]^+$); ES− 144.8 (100% − PF_6^-), 474.4 (5% − $[P_{17}(PF_6)_2]^-$).

Single-Crystal X-ray Crystallography. Colorless crystals of $P_{11}I$ and $P_{1x}PF_6$ were covered in viscous oil, mounted on a glass fiber, and placed directly into the cold nitrogen stream on an Enraf Nonius CCD diffractometer. A sphere of data for each specimen was obtained (1° scans in ϕ) and merged to a unique data set using the Nonius proprietry software COLLECT and DENZO-SMN. The structures were solved by direct methods and refined by least squares using all F^2 data, with anisotropic thermal parameter forms for the non-hydrogen atoms. Hydrogen atoms were placed in calculated positions using a riding model and were not refined.

Results and Discussion

Thermal Properties. The thermal properties of the salts are summarized in Table 1. The dimethyl derivative ($P_{11}PF_6$) has a relatively high melting point (it decomposes at ~390 °C before melting). The melting points generally fall with increasing alkyl chain length,

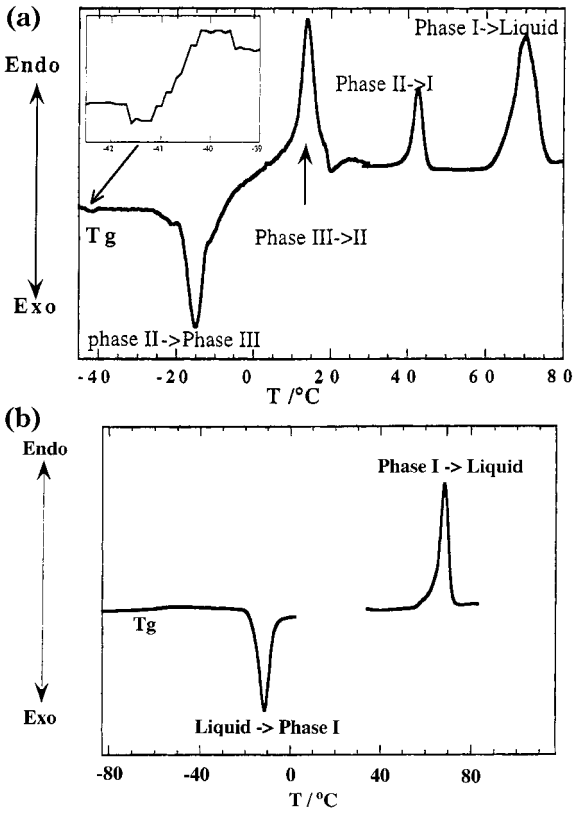

Figure 1. (a) Thermogram of *N*-methyl-*N*-butylpyrrolidinium hexafluorophosphate ($P_{14}PF_6$) showing the presence of multiple submelting phase transitions. The approximate equivalence of the areas of the exotherm around −15 °C and the endotherm at 14 °C suggests that the sample had quenched into the phase II glass. A small endotherm characteristic of a glass transition is observed around −41 °C (inset). (b) Thermogram of *N*-methyl-*N*-heptylpyrrolidinium hexafluorophosphate ($P_{17}PF_6$) showing behavior characteristic of the liquid sample having quenched directly into a fully amorphous state, passing through a glass transition on warming, followed by crystallization of phase I and then melting of this phase.

while the melting points for the PF_6^- salts are uniformly lower than the iodide salts (e.g. $P_{17}PF_6$ mp = 66 °C and $P_{17}I$ mp = 97 °C), with the exception of $P_{16}PF_6$. The pyrrolidinium cation and the PF_6^- anion are both relatively diffuse ions, which results in weak interactions between cation and anion. The iodide ion with its large polarizability and smaller size interacts more strongly with the cation, hence producing higher melting points.

The nomenclature used here denotes the highest temperature solid phase as phase I, with subsequent lower temperature phases denoted as phases II, III, etc.[11] The thermogram of $P_{14}PF_6$ (Figure 1a) shows the richest crystalline behavior of the family of compounds described here, with at least three solid phases (I−III) observed. We describe the thermal events in detail for this compound by way of example for the family as a whole. On quenching at the beginning of the thermal analysis experiment, the sample appears to form a, at least partially, glassy state showing a glass transition temperature around −42 °C. An exotherm appears at −15 °C which represents the crystallization of the supercooled phase II to a low-temperature phase (phase III). At 14 °C, phase III then transforms to the higher temperature phase (phase II). At 43 °C, phase II

Table 2. Crystal Data for $P_{1x}PF_6$ and Related Compounds

	$P_{11}I$[a]	Me_4NI[20]	$P_{11}PF_6$	Me_4NPF_6[21]	Me_3NetI[22]	Me_4NIO_4[23]
T (K)	123	295	233	170	300	293
a (Å)	7.1456(1)	7.955	8.889(1)	8.436(2)	8.430(5)	8.749
b (Å)	11.8436(2)	7.955	8.889(1)	8.436(2)	8.430(5)	8.749
c (Å)	10.53637(2)	5.747	6.419(1)	6.089(2)	6.216(4)	6.054
β (deg)	94.838(1)	90	90	90	90	90
V (Å^3)	873.9	364	507(2)	433	442(2)	463
Z	4	2	2	2	2	2
D (g cm^{-3})	1.73	1.56	1.61	1.68	1.617	
space gp	$P2_1/n$	$P4/nmm$	$P4/nmm$	$P4/nmm$	$P4/nmm$	$P4/nmm$

[a] R, R_w ($I > 2\sigma(I)$) = 0.017, 0.041. R, R_w (all data) = 0.018, 0.041.

transforms to phase I, which subsequently melts at 70 °C (entropy of fusion 13 J K^{-1} mol^{-1}). The approximate equivalence of the areas of the low-temperature exotherm and the III−II transition indicates that the exotherm represents the crystallization of phase III from a supercooled phase II and that therefore the glass transition observed at −42 °C corresponds to what we describe as the *phase II glass*. The phenomenon of multiple glassy states for a given plastic crystal compound is a fascinating phenomenon which will be discussed in more depth elsewhere; to summarize, each of the rotationally disordered phases in principle can be quenched into an arrested state, which on warming should exhibit a glass transition at the point where the motions involved become active. The glass transition temperatures of each of these arrested states may be different.

One of the criteria established by Timmermans[18] for the existence of a plastic crystal was that the entropy of melting of the plastic phase is generally < 20 J K^{-1} mol^{-1}. This was based on the observation that the molecular solids investigated by Timmermans had a low entropy of melting and exhibited one or more submelting solid−solid-phase transitions. In previous investigations of the plastic crystal behavior of similar salts, e.g. pyrrolidinium bis(trifluoromethanesulfonyl)amide salts,[6] MacFarlane and co-workers suggested that the entropy of melting of ionic plastic crystal phases might be higher than 20 J K^{-1} mol^{-1} for ionic materials where only one of the molecular ions is involved in the rotations and where both of the ions possess multiple degrees of rotational freedom. In the present case all of the salts which displayed solid−solid transitions and for which melting data could be determined had ΔS_f < 20 J K^{-1} mol^{-1}. Thus these compounds exhibit all of the classic features of plastic crystal formation. That the PF_6^- salts exhibit lower ΔS_f than the corresponding bis(trifluoromethanesulfonyl)amide salts[6] supports the argument that the internal degrees of freedom of the latter anion are responsible for the higher ΔS_f values and that the plastic crystal behavior in those compounds has its origin mainly in cation rotations.

The DSC trace of $P_{17}PF_6$ (Figure 1b) shows a glass transition around −60 °C followed by a crystallization at −10 °C and melting of this phase around 66 °C. The approximate equivalence of the enthalpies of crystallization and melting peaks indicates that the crystallization exotherm represents crystallization of phase I and that the glassy state quenched-in below this event is that of the fully amorphous liquid. There are no other

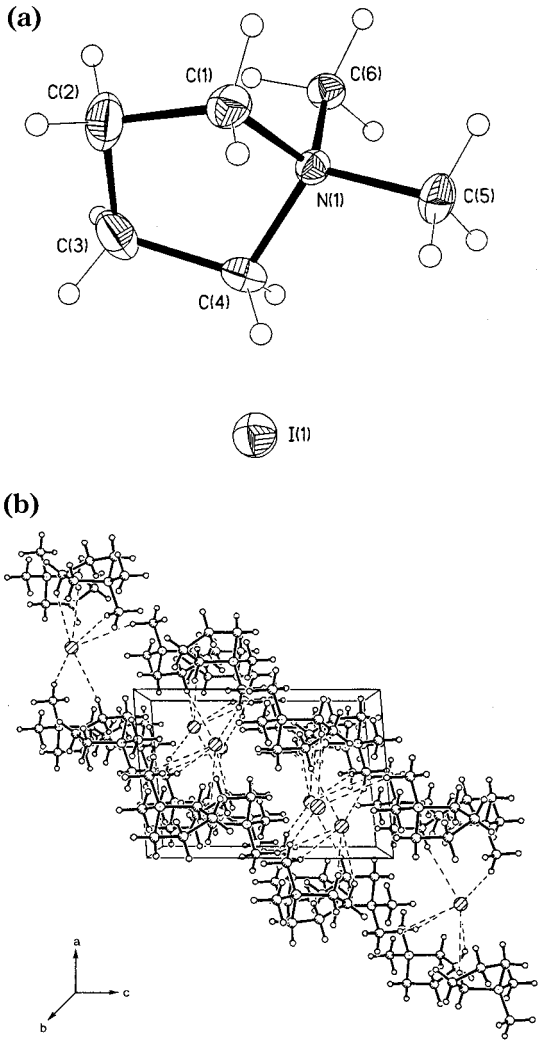

Figure 2. Crystal structure of *N*,*N*-dimethylpyrrolidinium iodide ($P_{11}I$) at 123 K: (a) unique ion pair (30% thermal ellipsoids); (b) packing diagram viewed along the *b* axis (weak H···I contacts shown with dashed lines).

solid−solid thermal transitions evident for this sample suggesting that, within the temperature regimes studied, only phase I exists. The ability to vitrify this sample is attributed to the decrease in symmetry of the pyrrolidinium-based cation with increase in substituent length. The size of the final entropy of melting is considerably greater than the other $P_{1x}PF_6$ materials (38 J K^{-1} mol^{-1}), which is consistent with the lack of submelting thermal transitions for this compound.

Attempts to melt $P_{11}PF_6$ were unsuccessful because of decomposition prior to melting. The thermogram of this salt is otherwise featureless except for a sharp

(18) Timmermans, J. *J. Phys. Chem. Solids* **1961**, 18.

Table 3. Selected Bond Distances and Angles

	$P_{11}I$	$P_{13}PF_6$	$P_{17}PF_6$
		Distances (Å)	
av N−C	1.505	1.504	1.509
range	1.497(3)−1.515(2)	1.464(7)−1.538(6)	1.49(1)−1.540(9)
av C−C	1.527	1.512	1.522
range	1.515(2)−1.524(3)	1.441(8)−1.57(2)	1.49(1)−1.56(1)
		Angles (deg)	
av ⌜C−N−C⌝	102.2(2)	102.2	102.8
range		101.4(8)−103.0(4)	102.1(6)−103.4(6)
av C−N−C	110.9	110.9	110.8
range	109.8(2)−112.0(2)	108.1(4)−113.4(6)	109.2(6)−112.5(6)
av ⌜C−C−C⌝	105.4	105.4	105.5
range	105.2(2)−105.6(2)	104.1(5)−106.3(4)	102.1(6)−107.8(8)
av C−C−C		109.9	113.0
range		107.8(1)−111.6(4)	108.8(7)−119.6(8)
		Distances (Å)	
av P−F		1.588	1.600
range		1.543(4)−1.606(3)	1.580(5)−1.624(5)
		Angles (deg)	
av F−P−F(trans)		178.8	178.3
range		176.5(3)−180.0	177.4(4)−179.5(3)
av F−P−F(cis)		90.0	90.0
range		87.2(3)−93.8(2)	86.7(3)−93.0(3)

endotherm at −50 °C which is assigned to a solid−solid-phase transition (II → I).

Single-Crystal X-ray Diffraction Studies. Several of the *N*-methyl-*N*-alkylpyrrolidinium hexafluorophosphate salts and also, for comparison, *N*,*N*-dimethylpyrrolidinium iodide were examined by single-crystal X-ray diffraction methods. Colorless crystals of $P_{11}I$ were grown by the diffusion of diethyl ether into an acetonitrile solution of the iodide salt, while the PF_6^- salts (P_{11}, P_{13}, P_{17}) were grown by slow evaporation of saturated aqueous solutions. The iodide formed clear regular prisms, and data, collected at both 293 and 123 K, indexed to a monoclinic unit cell (Table 2). This invariance with temperature indicates that no significant structural changes occur on cooling. Structure solution of the low-temperature data revealed discrete P_{11}^+ cations and I^- anions (Figure 2a) with one ion pair comprising the asymmetric unit. Bond distances and angles within the P_{11}^+ cation are listed in Table 3. The extended structure, when viewed down the *b* axis (Figure 2b) shows a two-dimensional layered superstructure of alternating regions of P_{11}^+ cations and I^- anions parallel to the 101 plane. In this low-temperature state, there are weak H···I interactions (average 3.10 Å between the cation and anion regions). The cations stack in the *b* direction in columns, 4 columns passing through each 001 plane, the C(12) (or C(9)) interleaving between pairs of columns. A similar layered structure has been observed for the 1-ethyl-3-methylimidazolium iodide system with cations and anions stacked in alternate layers.

$P_{11}PF_6$ formed clear hexagonal shaped crystals, but unlike the $P_{11}I$ crystals which were brittle and could be cleaved along the crystal planes, the $P_{11}PF_6$ crystals were soft and readily deformable. This indicates that the crystals may be in a plastic phase. Sharp X-ray diffraction maxima were observed at 233 K, which is above the phase II → phase I transition and thus corresponds to the phase I state. Data collected at this temperature indexed to a tetragonal cell (Table 2), similar to that of NMe_4PF_6, in which both the cation and anion are ordered. An example of isostructural pyrrolidinium and tetramethylammonium salts has previously been noted in the $R_4NOH{\cdot}2H_2O$ (R_4N = Me_4N or P_{11}) systems.[24] A preliminary structure solution of the data in the 4/*nmm* space group was consistent with the Me_4NPF_6 structure, the PF_6 anion being located on the 4-fold axis and the nitrogen atom situated on the $\bar{4}$ position at 0.75, 0.25, 0. However, the β ring carbons of the P_{11}^+ cation could not be located, and refinement of the structural model was unsatisfactory (see Supporting Information). Tetragonal unit cells, similar to that found for the $P_{11}PF_6$, are also observed for salts of NC_4-based cations in dynamically disordered (phase I) phases, e.g., $[Me_3NEt][I]$ (Table 2) where it has been proposed that the cation exhibits anisotropic motion, and $[Me_4N][IO_4]$ (Table 2) which has been modeled with the IO_4^- rotationally disordered about one I−O axis. Since the P_{11}^+ cation has a lower than $\bar{4}$ symmetry, the current model requires the cation to be extensively disordered. In particular the cation is required to be rotationally disordered about one or more axes passing through the nitrogen. Refinement in lower symmetry crystal lattices did not improve the structural model. Thus, the results are consistent with the phase I of the $P_{11}PF_6$ also being an anisotropically disordered phase resulting from cation (and possibly also anion) motion.

On further cooling of the $P_{11}PF_6$ crystal, a sharp change in the diffraction pattern was observed between 208 and 203 K, corresponding to crystallization of the

(19) Abdul-Sada, A. K.; Greenway, A. M.; Hitchcock, P. B.; Mohammed, T. J.; Seddon, K. R.; Zora, J. A. *J. Chem. Soc., Chem. Commun.* **1986**, *24*, 1753−4.
(20) Herrschaft, G.; Hartl, H. *Acta Crystallogr., Sect.C* **1989**, *45*, 1021.
(21) Wang, Y.; Calvert, L. D.; Browntein, S. K. *Acta Crystallogr., Sect. B* **1980**, *36*, 1523.
(22) Ishida, H.; Furukawa, Y.; Kashino, S.; Sato, S.; Ikeda, R. *Ber. Bunsen-Ges. Phys. Chem.* **1996**, *100*, 433.
(23) Wagner, R. I.; Bau, R.; Gnann, R. Z.; Jones, P. F.; Christie, K. O. *Inorg. Chem.* **1997**, *36*, 2564.
(24) Stäben, D.; Dahlems, Th.; Mootz, D. *Z. Kristallogr.* **1998**, *213*, 199.

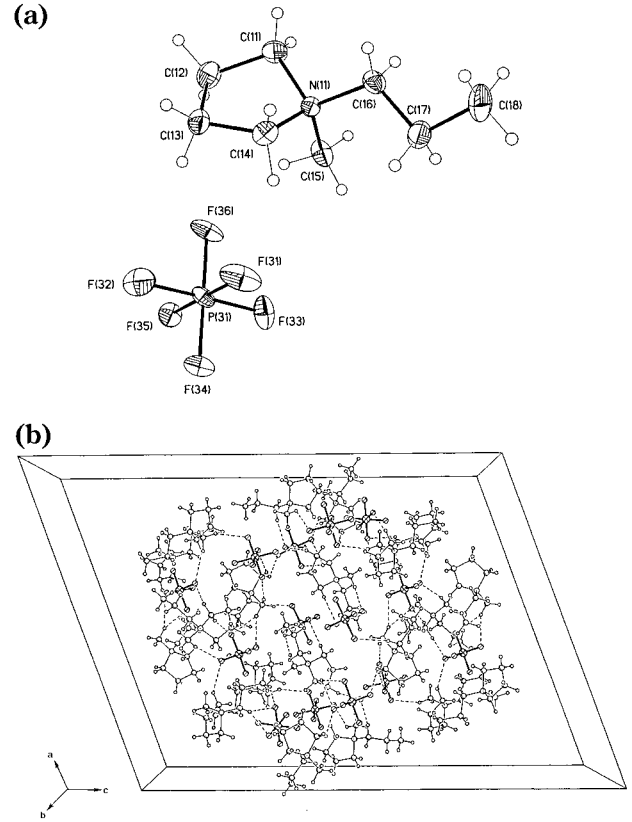

Figure 3. Crystal structure of *N*-methyl-*N*-propylpyrrolidinium hexafluorophosphate ($P_{13}PF_6$) at 123 K: (a) one of the unique ion pairs (30% thermal ellipsoids); (b) packing diagram viewed along the *b* axis (weak H···F contacts shown with dashed lines; disordered components of the cations omitted for clarity).

Table 4. Crystal Data for $P_{1x}PF_6$ Compounds

	$P_{13}PF_6$	$P_{17}PF_6$
T (K)	123	123
a (Å)	25.0964(7)	8.0793(2)
b (Å)	13.5788(5)	14.6031(4)
c (Å)	34.0634(13)	13.7634(3)
β (deg)	109.78(2)	91.070(1)
V (Å^3)	10922(4)	1623.6(6)
Z	36	4
space gp	*C*2/*c*	$P2_1$
R_1, R_w ($I > 2\sigma(I)$)	0.078, 0.199	0.071, 0.202
R_1, R_w (all data)	0.124, 0.232	0.102, 0.220

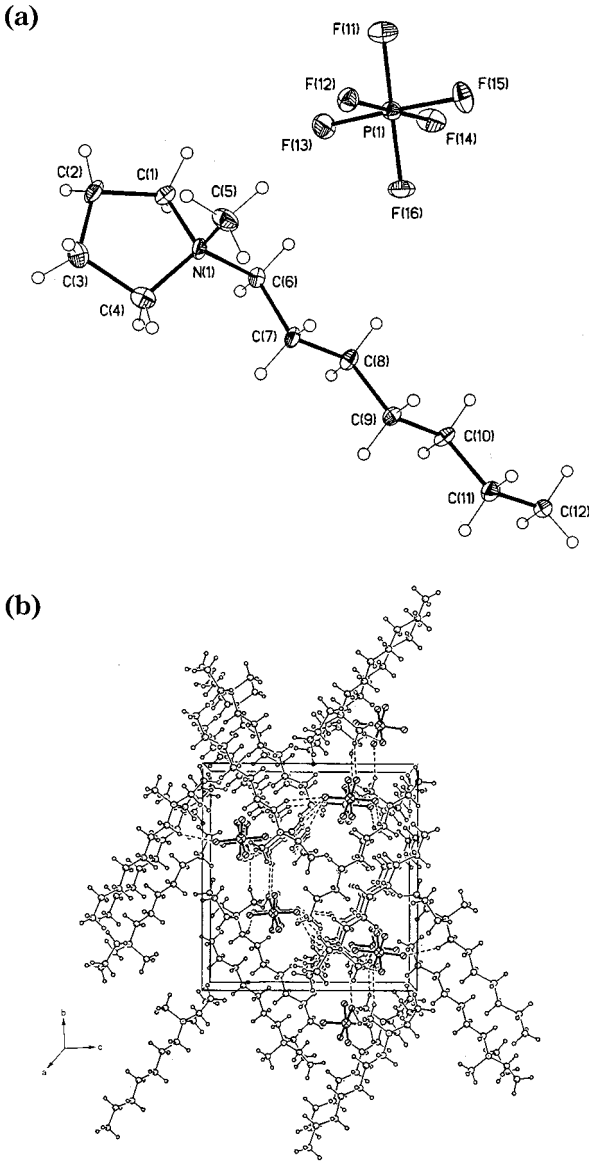

Figure 4. Crystal structure of *N*-methyl-*N*-heptylpyrrolidinium hexafluorophosphate ($P_{17}PF_6$) at 123 K: (a) one of the unique ion pairs (30% thermal ellipsoids); (b) packing diagram viewed along the *a* axis (weak H···F contacts shown with dashed lines).

supercooled phase I to phase II. This change was reversible on warming, but the transition occurred near 223 K, consistent with the DSC data. Unfortunately, the diffraction maxima of the low temperature phase were badly split, precluding satisfactory lattice indexing, and attempts to anneal the sample produced only minor improvements. Since ordered phases of Me_4NI[20] and Me_4NPF_6[21] (Table 2) are closely related, it could be anticipated that the low-temperature structure of P_{11}-PF_6 may be similar to that of the $P_{11}I$ (above). The splitting of the data in the low-temperature phase may be the result of the nucleation and growth of differently oriented phase II crystallites in the single crystal of phase I. Presumably this problem could be avoided by the preparation of a single crystal directly at 200 K. At room temperature the diffraction data was consistent with the 223 K tetragonal unit cell.

Small cubes of $P_{13}PF_6$, free from major imperfections, were cut from larger, irregularly shaped crystals and cooled to 123 K. Presumably, at this temperature, the crystal represents an arrested phase I state, phase I being the room-temperature-stable state. The low-temperature diffraction data for $P_{13}PF_6$ indexed to a rather large monoclinic cell (Table 4), and subsequent structure solution in the space group *C*2/*c* revealed 36 ion pairs of $P_{13}PF_6$ in the unit cell. The asymmetric component comprised 4 pairs of ions, in addition to a PF_6 situated on an inversion center (0.25, 0.25, 0) with the corresponding P_{13} cation modeled as disordered about the 2-fold axis with occupancies set at 0.5. Both isomers of the P_{13} cation are present in the asymmetric unit, but the bond distances and angles of the individual $P_{13}PF_6$ ion pairs are similar (Table 3). There was no indication of the presence of water of crystallization, as was observed for $P_{11}OH{\cdot}2H_2O$.[24] The final residual electron density peaks were only found in the vicinity of some of the phosphorus atoms indicating that there is little possibility of unidentified water in this struc-

ture. In fact this residual may possibly be associated with partial disorder in the PF_6 ions. The extended structure, when viewed down the *b* axis (Figure 3), is similar to that of $P_{11}I$ with alternating regions of P_{13} cations and PF_6 anions. In this low-temperature state there are weak H···F interactions (average separation = 2.40 Å) between the cation and anion regions.

As for $P_{13}PF_6$, a smaller crystal of $P_{17}PF_6$ was cut from a larger cluster of prismatic crystals and quenched to 123 K, corresponding to a quenched phase I state. The data indexed to a smaller monoclinic cell (Table 4) than for $P_{13}PF_6$ despite the larger cation. Structure solution in the noncentrosymmetric space group $P2_1$ showed two independent but similar $P_{17}PF_6$ ion pairs (one of which is shown in Figure 4a). Only one enantiomer is present; however, the absolute configuration could not be reliably determined from the current data. The bond distances and angles (Table 3) are similar in the two ion pairs and also similar to the corresponding parameters in $P_{13}PF_6$. The P_{17} cations pack in the crystal in a groups of two with parallel C_7 chains, and these groups are then rotated with respect to each other to give a pseudo-network superstructure, with the PF_6 anions located in voids within the network (Figure 4b). There are also weak H···F interactions between the anion and cation. Diffraction data were obtained at room temperature from the same crystal. Considerably fewer diffraction peaks were observed, although the derived unit cell parameters were not inconsistent with the low-temperature structure; however, the fit was less satisfactory. This loss of diffraction peaks at room temperature, while the crystal system remains unchanged, indicates the likely presence of increased molecular motions at room temperature. The structures of the $P_{13}PF_6$ and $P_{17}PF_6$ crystals clearly show the effect of increasing the length of the alkyl chain. The network P_{17} cations would be expected to have considerably more restricted motion, leading to the presence of only a single ordered phase of $P_{17}PF_6$ prior to melting, whereas the P_{13} (and P_{11}) should have greater rotational freedom, ultimately leading to the dynamically disordered room-temperature phase of $P_{11}PF_6$.

Summary and Conclusions

A new family of salts, based on the *N*-methyl-*N*-alkylpyrrolidinium cation and PF_6^-, were formed by metathesis of the pyrrolidinium iodide salt. The smaller, more symmetrical salts ($P_{11}PF_6$ and $P_{12}PF_6$) exhibited the highest melting points. The PF_6^- anion was found to depress the melting points in all but one of the salts when compared to the iodide anion. The melting point was generally found to fall with the increase of the alkyl chain length. Several of the compounds showed sub-melting phase transitions which, in conjunction with a correspondingly low entropy of fusion, suggests that these compounds are entering plastic crystal phases before melting. Single-crystal X-ray diffraction data and crystal structure solutions obtained for several of the salts at various temperatures confirm that the salts exhibit various stages of rotational motion of both the cation and anion in the case of $P_{11}PF_6$ and $P_{13}PF_6$. These observations are consistent with those described previously in the case of the tetraalkylammonium-based plastic crystal systems. The X-ray data also support the description of the higher temperature phases encountered in several compounds in this work as plastic crystals. On this basis, we can now begin to understand the high ionic conductivity of these systems; the combination of rotational/translational disorder with the layered structure seen here would lead to relatively facile ionic motions. Conductivities of these compounds and their Li salt mixtures will be discussed elsewhere.

Acknowledgment. The authors gratefully acknowledge funding from the Australian Research Council for this work.

Supporting Information Available: Details of the X-ray structure determinations of $P_{13}PF_6$ and $P_{17}PF_6$, including tables of final coordinates, thermal parameters, and full bond distances and angles (PDF). This material is available free of charge via the Internet at htpp://pubs.acs.org. Complete structural data are also available from the Cambridge Crystallographic Data Centre as supplementary publication Nos. CCDC 151365-151367.

CM000625W